

Three-dimensional contrast transfer functions in propagation-based tomography

Darren Thompson^{a,b}, Yakov I. Nesterets^a, Konstantin M. Pavlov^{c,d,b} and Timur E. Gureyev^{e,d}

^a Commonwealth Scientific and Industrial Research Organisation, Clayton, Victoria, Australia

^b University of New England, Armidale, New South Wales, Australia

^c University of Canterbury, Christchurch, New Zealand

^d Monash University, Clayton, Victoria, Australia

^e The University of Melbourne, Parkville, Victoria, Australia

Abstract

A single-step method is developed for three-dimensional reconstruction of the spatial distribution of complex refractive index in weakly scattering objects from multiple planar transmission images. The images are collected using coherent or partially-coherent illumination at a range of incident directions in the Fresnel region after free-space propagation from the object to the detector. The method is based on the contrast transfer function formalism extended to the cases of partially-coherent illumination and strongly absorbing samples. The proposed tomographic methods can be used for 3D reconstruction of internal structure of objects with X-rays, electrons and other forms of radiation and matter waves. Compared to related previously published methods for propagation-based phase-contrast tomography, the results reported in the present paper can be applied to a wider range of imaging conditions and can be also advantageous in terms of computational efficiency and robustness with respect to noise.

Keywords: phase contrast, computed tomography, contrast transfer functions, three-dimensional reconstruction

OCIS codes:

1. Introduction

We recently proposed a method for a single-step three-dimensional (3D) reconstruction of the internal structure of objects in propagation-based X-ray phase-contrast tomography (PB-CT) (Thompson *et al.*, 2019). This method was based on the combination of conventional computed tomography (CT) with phase retrieval using the Transport of Intensity equation (TIE) (Teague, 1983). As such, the method was applicable to the so-called "near-Fresnel" imaging conditions, i.e. the cases where the Fresnel number is much larger than unity: $N_F \equiv h^2 / (\lambda R) \gg 1$, where h is the size of the imaged feature of interest, λ is the radiation wavelength and R is the effective free-space propagation distance between the imaged object and the detector (Gureyev *et al.*, 2004). In the present paper, we extend this method to the whole of the Fresnel region, including the "far-Fresnel" zone, where $N_F \ll 1$. The latter imaging conditions can be encountered in practice, for example, in X-ray imaging (Mayo *et al.*, 2003) or electron microscopy (Cowley, 1995). Mathematically, the principal difference between the method proposed in (Thompson *et al.*, 2019) and the one developed in the present paper, can be explained in terms of the corresponding approaches to the linearization (with respect to the refractive index, $n(\mathbf{r}) = 1 - \Delta(\mathbf{r}) + i\beta(\mathbf{r})$, of the imaged object) of the general image intensity distribution expressed by the square modulus of the Fresnel diffraction integral. The method in (Thompson *et al.*, 2019), being based on the TIE, uses a linearization relying on the slow spatial variation of the refractive index. In contrast, the method developed in the present paper is based initially on the assumption of the weak scattering (first Born approximation), which assumes that the deviation of the refractive index from unity is small (see details in the next section). This approach is known as the contrast transfer function (CTF) or Fourier optics theory (Cowley, 1995; Pogany *et al.*, 1997). However, we subsequently show that, following the ideas described in (Wu & Liu, 2003; Gureyev *et al.*, 2004; Guigay *et al.*, 2007; Nesterets & Gureyev, 2016; Gureyev & Nesterets, 2017), the two approaches can be merged, leading to a solution that is valid for refractive index distributions that can be represented as a sum of a slowly varying and a small components.

Considering another key aspect of the problem of the reconstruction of the 3D distribution of the complex refractive index inside an object from transmission images collected at different incident illumination directions (or object orientations), we note that the conventional approach used for solution of this problem in the case of weakly absorbing objects consists essentially of two stages. At the first stage, the collected 2D images are processed with the goal of recovering the phase distribution of the transmitted beam from the registered intensity distribution(s) (Gureyev *et al.*,

2004), subsequently “back-propagating” the resultant complex amplitudes from the image (detector) plane to the object plane at each illumination direction. At the second stage, the distributions of the complex amplitude in the object planes, obtained at different illumination directions, are processed together to reconstruct the 3D distribution of the complex refractive index in the object by means of conventional CT techniques (Natterer, 2001). The approach described in (Thompson *et al.*, 2019) allows one to effectively merge these two stages into a single step, which may have advantages in terms of the computational efficiency and robustness. Related versions of single-step PB-CT reconstruction were also described in earlier publications (Bronnikov, 1999; Bronnikov, 2002; Gureyev *et al.*, 2006). The methods developed in the present paper also belong to this type of single-step 3D reconstruction from phase-contrast projections, with the difference from the previously considered cases being primarily in the broader object classes and imaging conditions under which the projections are collected (as explained above).

In the two-stage PB-CT algorithms, typically, the phase retrieval is applied first, in 2D, at each illumination angle, followed by the 3D CT reconstruction. In contrast, in the 3D PB-CT methods described in (Thompson *et al.*, 2019) and in the present paper, the 3D CT reconstruction is effectively applied to the “raw” phase-contrast images first and the phase retrieval is applied in 3D after that, even though the two operations appear as parts of a single analytical expression. As explained in (Thompson *et al.*, 2019), the latter methodology can be substantially advantageous e.g. in the case of objects containing several distinct components, each spatially localized to a 3D area Ω_m , with different locally-constant ratios $\gamma_m \equiv \Delta(\mathbf{r}) / \beta(\mathbf{r})$, $\mathbf{r} \in \Omega_m$, of the real decrement and the imaginary part of the complex refractive index (Beltran *et al.*, 2010). In this case, the computationally expensive 3D CT reconstruction step can be performed only once for the whole object volume, followed by repeated phase retrieval operations localized to different (smaller) 3D areas Ω_m . A highly efficient and stable 3D phase retrieval method based on the monomorphous (homogeneous) TIE (TIE-Hom) (Paganin *et al.*, 2002) can be applied here locally in Ω_m with the constant value γ_m . As will become obvious in the next section, a very similar methodology can be applied using the results derived in the present paper, with the straightforward replacement of the TIE-Hom phase retrieval by the corresponding monomorphous version of the 3D CTF (CTF-Hom) based phase retrieval. In the general case, the main results of the present paper can be applied to weakly scattering objects with arbitrary distribution of the complex refractive index. In order to make the phase retrieval possible in this general case, it is usually necessary to collect two or more images at different object-to-detector distances at each illumination direction (view angle); alternatively, two or more images can be collected at the same object-to-detector distance, but at different radiation wavelengths (Gureyev *et al.*, 2004). Compared to the reconstruction methods conventionally used in PB-CT in such a context,

the method developed below can provide some advantages in terms of computational efficiency and stability, in the same way as described previously in (Thompson *et al.*, 2019).

2. 3D CTFs for weakly scattering objects

Consider the PB-CT imaging system schematically shown in Fig. 1. Let an object be illuminated by a monochromatic plane X-ray wave with wavelength λ and intensity I_{in} , $I_{in}^{1/2} \exp(ikz')$ with $k = 2\pi / \lambda$. The image of the object is recorded on a position-sensitive detector located at the distance R downstream from the object. In the following we assume that the dimensions of the object are small compared to the source-to-object distance ρ and $\rho \ll R$. Interactions of the X-rays and object matter are described via the spatial distribution of the complex refractive index, $n(\mathbf{r}) = 1 - \Delta(\mathbf{r}) + i\beta(\mathbf{r})$, $\mathbf{r} = (x, y, z)$.

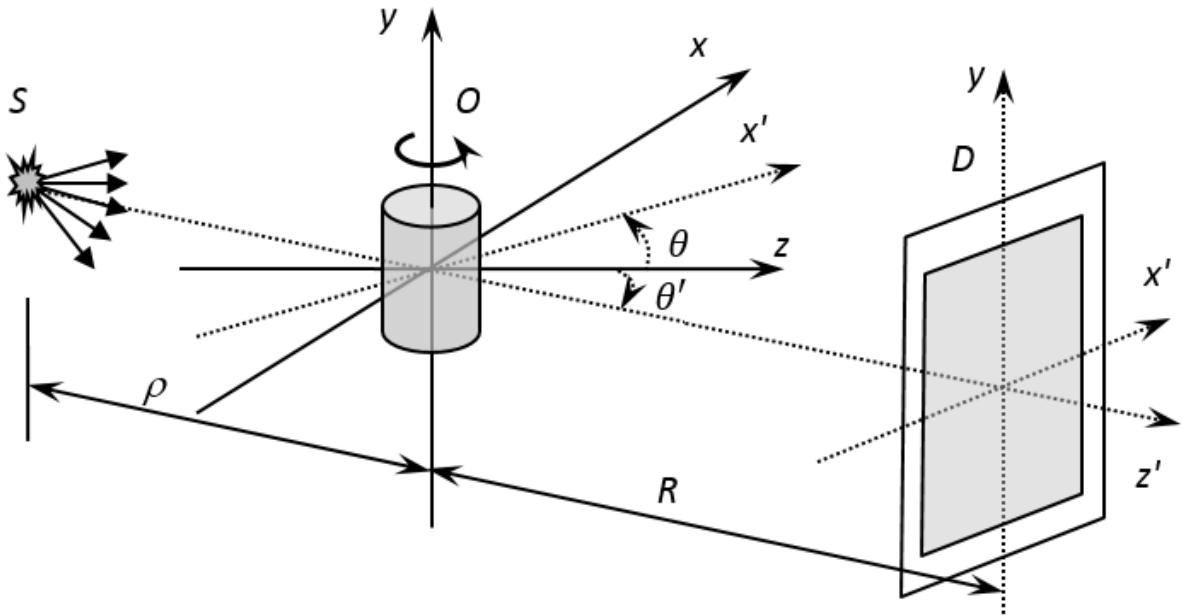


Figure 1 PB-CT experimental setup, the direction of the incident X-ray wave forms an angle θ' with the z axis, $-\pi/2 \leq \theta' < \pi/2$, and $\theta = \theta' + \pi/2$, the object and detector planes are located at $z'=0$ and $z'=R$ respectively.

Conventional X-ray radiography and CT are generally concerned with measuring the intensity distribution of transmitted radiation in the object plane and reconstructing the imaginary part of the complex refractive index, β , relating the attenuation characteristics of the object to the measured

intensity. In contrast, PB-CT seeks to utilise transmitted wavefront phase modulation resulting in visible diffraction fringes created upon propagation through a given distance. By processing this diffraction intensity pattern, phase information in the object plane can be mathematically retrieved.

In the following we assume that the interaction of the incident X-rays and object is accurately described by the complex scalar transmission function,

$$q_\theta(x', y) = \exp[-B_\theta(x', y) + i\varphi_\theta(x', y)], \quad (1)$$

consisting of the amplitude attenuation $B_\theta(x', y) = k\mathbf{P}_\theta\beta(x', y)$ and phase $\varphi_\theta(x', y) = -k\mathbf{P}_\theta\Delta(x', y)$ functions, both of which are defined in terms of the projection operator,

$$\mathbf{P}_\theta f(x', y) = \int_{-\infty}^{\infty} \int_{-\infty}^{\infty} f(x, y, z) \delta(x' - x \sin \theta - z \cos \theta) dx dz, \quad (2)$$

where δ represents the Dirac delta function.

The evolution of a paraxial transmitted wave in the free half-space $z' > 0$ can be described by the 2D Fresnel diffraction integral (Goodman, 2005),

$$\psi_\theta^R(x', y) = \frac{\exp(ikR)}{i\lambda R} \int_{-\infty}^{\infty} \int_{-\infty}^{\infty} \exp\left\{\frac{i\pi}{\lambda R}[(x' - x'')^2 + (y - y'')^2]\right\} q_\theta(x'', y'') dx'' dy''. \quad (3)$$

Equation (3) can be conveniently presented as the 2D convolution of the transmission function with the 2D Fresnel free-space propagator, $P_2^R(x', y) = (i\lambda R)^{-1} \exp[i\pi(x'^2 + y^2)/(\lambda R)]$,

$$\psi_\theta^R(x', y) = \exp(ikR) (P_2^R * q_\theta)(x', y).$$

Hereafter, the asterisk denotes the convolution of two functions, e.g. in the considered 2D case

$$(f * g)(x, y) = \int_{-\infty}^{\infty} \int_{-\infty}^{\infty} f(x', y') g(x - x', y - y') dx' dy'.$$

The spatial distribution of the propagated intensity in the detector plane is thus,

$$I_\theta^R(x', y) = |\psi_\theta^R(x', y)|^2. \quad (4)$$

The Fourier transform of the image intensity in eq.(4), derived by Guigay (Guigay, 1977) and extended to 2D from the original 1D case is given by,

$$\begin{aligned} \mathbf{F}_2 I_\theta^R(\xi', \eta) &= \int_{-\infty}^{\infty} \int_{-\infty}^{\infty} \exp[-i2\pi(x'\xi' + y\eta)] \\ &\times q_\theta\left(x' - \frac{1}{2}\lambda R\xi', y - \frac{1}{2}\lambda R\eta\right) q_\theta^*\left(x' + \frac{1}{2}\lambda R\xi', y + \frac{1}{2}\lambda R\eta\right) dx' dy, \end{aligned} \quad (5)$$

where the superscript asterisk denotes the complex conjugate and the 2D Fourier transform is defined as follows (note that the definition of the Fourier transform differs from one used in some of our recent papers),

$$\mathbf{F}_2 g(\xi', \eta) = \int_{-\infty}^{\infty} \int_{-\infty}^{\infty} \exp[-i2\pi(x'\xi' + y\eta)] g(x', y) dx' dy.$$

The phase retrieval problem is that of finding a solution to the non-linear eqs.(4) or (5) with respect to q_θ . To simplify this task, linearized approximations are generally desired for which many methods have been derived.

The linearization known as the CTF approximation, originally developed by Guigay (Guigay, 1977), can be derived under the assumptions of weak object attenuation and weak or slowly-varying phase:

$$\begin{cases} B_\theta(x', y) \ll 1, \\ |\varphi_\theta(x' - \lambda R\xi', y - \lambda R\eta) - \varphi_\theta(x', y)| \ll 1. \end{cases} \quad (6)$$

Applying these assumptions in addition to a uniform incident intensity distribution I_{in} in the object plane, Guigay obtained the linearized expression for the propagated intensity distribution (extended to the 2D case), *cf.* (Guigay, 1977)

$$\mathbf{F}_2 I_\theta^R(\xi', \eta) \cong I_{in} \begin{cases} \delta(\xi', \eta) - 2\mathbf{F}_2 B_\theta(\xi', \eta) \cos[\pi\lambda R(\xi'^2 + \eta^2)] \\ + 2\mathbf{F}_2 \varphi_\theta(\xi', \eta) \sin[\pi\lambda R(\xi'^2 + \eta^2)] \end{cases}. \quad (7)$$

Recall that the mathematical basis for CT can be described by the inversion equation,

$$\Re \mathbf{F}_2 \mathbf{P}_\theta f(x, y, z) = f(x, y, z), \quad (8)$$

where \Re is the filtered back-projection (FBP) operator,

$$\Re h(x, y, z) = \int_0^\pi \int_{-\infty}^{\infty} \int_{-\infty}^{\infty} \exp\{i2\pi[\xi'(x \sin \theta + z \cos \theta) + \eta y]\} h(\xi', \eta, \theta) |\xi'| d\xi' d\eta d\theta.$$

A generalised form of the 2D Fourier derivative theorem (Paganin, 2006) is given by,

$$\mathbf{F}_2 \left[\frac{\partial^m}{\partial x'^m} \frac{\partial^n}{\partial y^n} g(x', y) \right] (\xi', \eta) = (2\pi i \xi')^m (2\pi i \eta)^n \mathbf{F}_2 g(\xi', \eta). \quad (9)$$

Using eq.(9), an explicit form of the Fourier transform of the 2D Laplacian of a function in the detector plane can thus be expressed as the identity,

$$\mathbf{F}_2 \nabla_\perp^2 g(\xi', \eta) = -4\pi^2 (\xi'^2 + \eta^2) \mathbf{F}_2 g(\xi', \eta), \quad (10)$$

where $\nabla_\perp = \left(\frac{\partial}{\partial x'}, \frac{\partial}{\partial y} \right)$.

Moreover, when the 3D Laplacian is applied to both sides of eq.(8), the following equality can be established,

$$\Re \mathbf{F}_2 \nabla_{\perp}^2 \mathbf{P}_{\theta} f(x, y, z) = \nabla^2 f(x, y, z). \quad (3)$$

Here $\nabla = \left(\frac{\partial}{\partial x}, \frac{\partial}{\partial y}, \frac{\partial}{\partial z} \right)$.

Also, eqs.(10) and (11) can be easily generalised for any positive integer power n of the Laplacian,

$$\mathbf{F}_2 \nabla_{\perp}^{2n} g(\xi', \eta) = \left[-4\pi^2 (\xi'^2 + \eta^2) \right]^n \mathbf{F}_2 g(\xi', \eta), \quad (12)$$

$$\Re \mathbf{F}_2 \left(\nabla_{\perp}^2 \right)^n \mathbf{P}_{\theta} f(x, y, z) = \left(\nabla^2 \right)^n f(x, y, z). \quad (13)$$

Importantly, this last property, eqs.(11) and (13), demonstrates the ability to switch the order of differentiation and filtered back-projection, with the noticeable change of the dimensionality of the Laplacian operator between 2D projections and the reconstructed volume in 3D real space. A post CT-reconstruction method for phase retrieval of monomorphous objects in the TIE regime has been derived (Thompson *et al.*, 2019) exploiting this property.

Below, we adapt this approach for the CTF approximation by expressing the Fresnel propagator components in terms of a Laplacian to utilise relationship in eq.(13).

Let $K_{R,\theta}(x', y) \square 1 - I_{\theta}^R(x', y) / I_{in}$ designate the in-line contrast function, with

$\mathbf{F}_2 P_2^a(\xi', \eta) = \cos[\pi\lambda R(\xi'^2 + \eta^2)]$ and $\mathbf{F}_2 P_2^p(\xi', \eta) = -\sin[\pi\lambda R(\xi'^2 + \eta^2)]$ being the 2D Fourier transforms of the amplitude and phase Fresnel propagators respectively (Nesterets & Gureyev, 2014).

Rearranging eq.(7) produces the expression,

$$\mathbf{F}_2 K_{R,\theta}(\xi', \eta) = 2\mathbf{F}_2 B_{\theta}(\xi', \eta) \mathbf{F}_2 P_2^a(\xi', \eta) + 2\mathbf{F}_2 \varphi_{\theta}(\xi', \eta) \mathbf{F}_2 P_2^p(\xi', \eta). \quad (14)$$

The 2D Fourier transform of the amplitude Fresnel propagator, $\mathbf{F}_2 P_2^a(\xi', \eta)$, when expressed as a Taylor series has the form,

$$\mathbf{F}_2 P_2^a(\xi', \eta) = \sum_{n=0}^{\infty} \frac{(-1)^n}{(2n)!} \left[\pi\lambda R(\xi'^2 + \eta^2) \right]^{2n}. \quad (15)$$

Multiplying the expansion by the Fourier transform of the 2D projection, $\mathbf{F}_2 \mathbf{P}_{\theta} f(\xi', \eta)$, leads to,

$$\mathbf{F}_2 P_2^a(\xi', \eta) \mathbf{F}_2 \mathbf{P}_{\theta} f(\xi', \eta) = \sum_{n=0}^{\infty} \frac{(-1)^n}{(2n)!} \left[\pi\lambda R(\xi'^2 + \eta^2) \right]^{2n} \mathbf{F}_2 \mathbf{P}_{\theta} f(\xi', \eta). \quad (16)$$

Using eq.(12) the right-hand side of eq.(16) can be re-written in terms of the power series of the Laplacian of projections,

$$\mathbf{F}_2 \mathbf{P}_2^a(\xi', \eta) \mathbf{F}_2 \mathbf{P}_\theta f(\xi', \eta) = \sum_{n=0}^{\infty} C_n^a \mathbf{F}_2 \left\{ \left[\nabla_{\perp}^2 \right]^{2n} \mathbf{P}_\theta f \right\}(\xi', \eta), \quad (17)$$

where $C_n^a = \frac{(-1)^n}{(2n)!} \left[\frac{\lambda R}{4\pi} \right]^{2n}$.

It is worth noting that according to eq.(17) the amplitude contrast (this corresponds to the first term in the right-hand side of eq.(14)) can be expressed as a power series of the Laplacian of the attenuation function,

$$(\mathbf{P}_2^a * \mathbf{B}_\theta)(x', y) = \sum_{n=0}^{\infty} C_n^a \left[\nabla_{\perp}^2 \right]^{2n} \mathbf{B}_\theta(x', y).$$

Similarly, the phase contrast (this corresponds to the second term in the right-hand side of eq.(14)) can be expressed as a power series of the Laplacian of the phase function,

$$(\mathbf{P}_2^p * \varphi_\theta)(x', y) = \sum_{n=0}^{\infty} C_n^p \left[\nabla_{\perp}^2 \right]^{2n+1} \varphi_\theta(x', y),$$

where the coefficients C_n^p are defined below, next to eq.(19).

Using eq.(13), the filtered back-projection operator applied to the right-hand side of eq.(17) is expressed as follows,

$$\Re \left(\sum_{n=0}^{\infty} C_n^a \mathbf{F}_2 \left\{ \left[\nabla_{\perp}^2 \right]^{2n} \mathbf{P}_\theta f \right\} \right)(x, y, z) = \sum_{n=0}^{\infty} C_n^a \Re \left(\mathbf{F}_2 \left[\nabla_{\perp}^2 \right]^{2n} \mathbf{P}_\theta f \right)(x, y, z) = \sum_{n=0}^{\infty} C_n^a \left[\nabla^2 \right]^{2n} f(x, y, z).$$

Hence,

$$\Re \left(\mathbf{F}_2 \mathbf{P}_2^a \mathbf{F}_2 \mathbf{P}_\theta f \right)(x, y, z) = \sum_{n=0}^{\infty} C_n^a \left[\nabla^2 \right]^{2n} f(x, y, z) = (\mathbf{P}_3^{a,R} * f)(x, y, z), \quad (18)$$

where we introduced a 3D amplitude propagator, $\mathbf{P}_3^{a,R}(x, y, z)$.

An equivalent treatment can be similarly applied to the phase component of the Fresnel propagator,

$$\mathbf{F}_2 \mathbf{P}_2^p(\xi', \eta) = -\sin \left[\pi \lambda R (\xi'^2 + \eta^2) \right], \text{ resulting in the equation,}$$

$$\mathbf{F}_2 \mathbf{P}_2^p(\xi', \eta) \mathbf{F}_2 \mathbf{P}_\theta f(\xi', \eta) = \sum_{n=0}^{\infty} C_n^p \mathbf{F}_2 \left\{ \left[\nabla_{\perp}^2 \right]^{2n+1} \mathbf{P}_\theta f \right\}(\xi', \eta),$$

where $C_n^p = \frac{(-1)^n}{(2n+1)!} \left[\frac{\lambda R}{4\pi} \right]^{2n+1}$.

Hence,

$$\Re \left(\mathbf{F}_2 \mathbf{P}_2^p \mathbf{F}_2 \mathbf{P}_\theta f \right)(x, y, z) = \sum_{n=0}^{\infty} C_n^p \left[\nabla^2 \right]^{2n+1} f(x, y, z) = (\mathbf{P}_3^{p,R} * f)(x, y, z), \quad (19)$$

where we introduced a 3D phase propagator, $P_3^{p,R}(x, y, z)$.

Applying the amplitude and phase reconstructions given by eqs.(18) and (19) to eq.(14), with proper substitutions for β and Δ , and expressing the result in 3D Fourier space results in,

$$\mathbf{F}_3 \Re \mathbf{F}_2 K_{R,\theta}(\xi, \eta, \zeta) = 2k \mathbf{F}_3 \beta(\xi, \eta, \zeta) \mathbf{F}_3 P_3^{a,R}(\xi, \eta, \zeta) - 2k \mathbf{F}_3 \Delta(\xi, \eta, \zeta) \mathbf{F}_3 P_3^{p,R}(\xi, \eta, \zeta), \quad (20)$$

where $\mathbf{F}_3 P_3^{a,R}(\xi, \eta, \zeta) = \cos[\pi \lambda R(\xi^2 + \eta^2 + \zeta^2)]$ and $\mathbf{F}_3 P_3^{p,R}(\xi, \eta, \zeta) = -\sin[\pi \lambda R(\xi^2 + \eta^2 + \zeta^2)]$ are the 3D Fourier transforms of the 3D amplitude and phase Fresnel propagators respectively and \mathbf{F}_3 represents the 3D Fourier transform operator,

$$\mathbf{F}_3 g(\xi, \eta, \zeta) = \int_{-\infty}^{\infty} \int_{-\infty}^{\infty} \int_{-\infty}^{\infty} \exp[-i2\pi(x\xi + y\eta + z\zeta)] g(x, y, z) dx dy dz. \quad (21)$$

3. Application of 3D CTFs for PB-CT reconstruction

Examination of the similarity between eqs.(14) and (20) establishes an important link between 2D and 3D expressions for propagation-based phase contrast in the CTF regime. Equation (20) represents a generalized form of 3D CTF phase contrast that provides a basis to reconstruct the complex refractive index in the object plane from post-FBP reconstructed propagation-based intensity measurements.

Moreover, with some algebraic manipulation, general solutions for the Fourier transforms of both β and Δ can be obtained for two propagation distances R_1 and R_2 (we have omitted the argument list (ξ, η, ζ) for the sake of conciseness):

$$\mathbf{F}_3 \beta = \frac{\Im_{R_2} \mathbf{F}_3 P_3^{p,R_1} - \Im_{R_1} \mathbf{F}_3 P_3^{p,R_2}}{2k \mathbf{F}_3 P_3^{p,R_1-R_2}}, \quad (22)$$

$$\mathbf{F}_3 \Delta = \frac{-\Im_{R_1} \mathbf{F}_3 P_3^{a,R_2} + \Im_{R_2} \mathbf{F}_3 P_3^{a,R_1}}{2k \mathbf{F}_3 P_3^{p,R_1-R_2}}. \quad (23)$$

Here $\Im_R(\xi, \eta, \zeta) = \mathbf{F}_3 \Re \mathbf{F}_2 K_{R,\theta}(\xi, \eta, \zeta)$ represents the 3D Fourier transform of the reconstructed in-line contrast function at the propagation distance R , see eq.(20).

The structure of eqs.(22) and (23) illustrates that both the real and imaginary parts of the refractive index decrement in the object plane can be retrieved by subtracting weighted 3D Fourier-filtered FBP reconstructions of the propagated intensity at two distances. Furthermore, absorption/phase retrieval can be performed after conventional FBP-CT reconstructions and, importantly, can be applied locally to a given CT-reconstructed sub-volume.

Assume that the object is monomorphous, such that a spatially independent (but energy-dependent) proportionality constant, $\gamma = \Delta / \beta$, holds for the complex refractive index (Paganin *et al.*, 2002, Mayo *et al.*, 2003). This assumption is valid, for example, for objects consisting of a single material and objects composed of light elements (with atomic numbers $Z < 10$) when irradiated with high-energy X-rays (60-500 keV).

Applying this property to the generalised CTF expression in eq.(20) provides a monomorphous form of the CTF, denoted CTF-Hom, allowing for the reconstruction of the object's complex refractive index from single set of intensity measurements collected at the propagation distance R ,

$$\beta(x, y, z) = \frac{1}{2k} \mathbf{F}_3^{-1} \left[\frac{\mathfrak{I}_R}{\mathbf{F}_3 P_3^{a,R} - \gamma \mathbf{F}_3 P_3^{p,R}} \right] (x, y, z), \quad (24)$$

Equation (24) implies that phase/amplitude retrieval can be implemented as a localisable 3D Fourier filter and applied as a post-CT reconstruction operation in the CTF regime for a monomorphous object acquired at a single propagation distance.

Moreover, it can be shown that the CTF-Hom reconstruction formula, eq.(24), reduces to the corresponding TIE form under the assumption that the transmission function, $q_\theta(x', y)$ is slowly varying on the length scale $\sqrt{\lambda R}$ at all θ whereby the in-line contrast function $K_{R,\theta}(x', y)$ is band-limited to the spectral region $\xi'^2 + \eta^2 \ll (\lambda R)^{-1}$. Applying these constraints to eq.(24) results in the cosine function (the amplitude propagator) reducing to 1 and the sine function (the phase propagator) being replaced by its argument giving the expression equivalent to that derived in (Thompson *et al.*, 2019),

$$\mathbf{F}_3 \beta(\xi, \eta, \zeta) = \mathfrak{I}_R(\xi, \eta, \zeta) / \left[2k + 4\pi^2 \gamma R (\xi^2 + \eta^2 + \zeta^2) \right]. \quad (25)$$

In its original form, the CTF approximation as derived above does not suffer constraints upon propagation distance as TIE approximations impose. However, it is quite restrictive due to the assumption of weak absorption, limiting its application to real-life imaging applications.

Subsequent works have extended the validity of the CTF by way of a “slowly-varying” object approximation allowing it to be used for absorbing objects (Wu & Liu, 2003; Gureyev *et al.*, 2004; Guigay *et al.*, 2007; Nesterets & Gureyev, 2016; Gureyev & Nesterets, 2017).

4. Extension to partially-coherent illumination and strongly absorbing objects

Nesterets (Nesterets & Gureyev, 2016) described an approximation of the CTF for partially coherent illumination with validity extended to strongly absorbing objects. An equivalent approach can be applied to extend the validity of 3D CTF.

Let the attenuation function be the sum of a small (“sm”), and a slowly varying (“sl”) components:

$$B_{\theta}(x', y) = B_{\theta,sm}(x', y) + B_{\theta,sl}(x', y). \quad (26)$$

It is assumed that small component satisfies $|B_{\theta,sm}(x', y)| \ll 1$ and $B_{\theta,sl}(x', y)$ varies slowly on the length scale relative to the width of the partially-coherent free-space propagator (Nesterets & Gureyev, 2016). Introducing the complex function,

$$\Phi(x', y) = -B_{\theta,sm}(x', y) + i\varphi_{\theta}(x', y), \quad (27)$$

and the contact intensity of the slowly varying attenuation component,

$$I_{\theta,sl}(x', y) = \exp[-2B_{\theta,sl}(x', y)], \quad (28)$$

the combined propagated intensity can be approximated as in (Nesterets & Gureyev, 2016):

$$I_{\theta}^R(x', y) \cong I_{in} I_{\theta,sl}(x', y) [1 + 2\text{Re}(\Phi * \tilde{P}_2^R)(x', y)]. \quad (29)$$

Here $\tilde{P}_2^R(x', y) = (P_2^R * P_{sys})(x', y)$ is the 2D partially-coherent Fresnel free-space propagator obtained by convolving the fully-coherent Fresnel free-space propagator with the point-spread function of the imaging system, $P_{sys}(x', y)$. The latter takes into account partial coherence of the incident illumination as well as finite resolution of the detector (Nesterets & Gureyev, 2016).

Rearranging eq.(29) by bringing the incident intensity to the left-hand side and applying the negative logarithm to both sides results in an expression representing the propagated contrast function:

$$\tilde{K}_{R,\theta}(x', y) \cong 2B_{\theta,sl}(x', y) - \log[1 + 2\text{Re}(\Phi * \tilde{P}_2^R)(x', y)], \quad (30)$$

with $\tilde{K}_{R,\theta}(x', y) = -\log\left(\frac{I_{\theta}^R(x', y)}{I_{in}}\right)$.

The logarithm on the right-hand side of eq.(30) can be linearized using the approximation $\log(1+x) \cong x$ as the contrast due to weak absorption and phase contrast are assumed to be small relative to unity,

$$\tilde{K}_{R,\theta}(x', y) \cong 2B_{\theta,sl}(x', y) + 2(B_{\theta,sm} * \tilde{P}_2^{a,R})(x', y) + 2(\varphi_\theta * \tilde{P}_2^{p,R})(x', y). \quad (31)$$

Here $\tilde{P}_2^{a,R}(x', y) = (P_2^{a,R} * P_{sys})(x', y)$ and $\tilde{P}_2^{p,R}(x', y) = (P_2^{p,R} * P_{sys})(x', y)$ are the 2D partially-coherent amplitude and phase Fresnel propagators, respectively.

Equation (31) represents a CTF approximation that is applicable and valid for strongly absorbing (but slowly varying) objects containing weakly absorbing features. Moreover, due to the above assumption that $B_{\theta,sl}$ varies slowly on the length scale relative to the width of the partially-coherent free-space propagator, the first two terms in the right-hand side of eq.(31) may be combined, such that

$B_{\theta,sl}(x', y) + (B_{\theta,sm} * \tilde{P}_2^{a,R})(x', y) \cong (B_\theta * \tilde{P}_2^{a,R})(x', y)$. Applying this simplification into eq.(31) results in,

$$\tilde{K}_{R,\theta}(x', y) \cong 2(B_\theta * \tilde{P}_2^{a,R})(x', y) + 2(\varphi_\theta * \tilde{P}_2^{p,R})(x', y), \quad (32)$$

which is equivalent to the CTF approximation given by eq.(14).

Applying the same 3D treatment to eq.(32) as we did with eq.(14) to derive eq.(20) provides an expression for the FBP reconstructed 3D contrast function which is similar to eq.(20),

$$\mathbf{F}_3 \Re \mathbf{F}_2 \tilde{K}_{R,\theta}(\xi, \eta, \zeta) \cong 2k\mathbf{F}_3 \beta(\xi, \eta, \zeta) \mathbf{F}_3 \tilde{P}_3^{a,R}(\xi, \eta, \zeta) - 2k\mathbf{F}_3 \Delta(\xi, \eta, \zeta) \mathbf{F}_3 \tilde{P}_3^{p,R}(\xi, \eta, \zeta). \quad (33)$$

Here $\tilde{P}_3^{a,R}(x', y) = (P_3^{a,R} * P_{3,sys})(x', y)$ and $\tilde{P}_3^{p,R}(x', y) = (P_3^{p,R} * P_{3,sys})(x', y)$ are the 3D partially-coherent amplitude and phase Fresnel propagators, respectively, and $P_{3,sys}(x, y, z)$ is the point-spread function of the imaging system in the reconstructed 3D volume.

Solutions of the 3D PB-CT reconstruction problem can be obtained from eq.(33) in exactly the same way as eqs.(22)-(24) were obtained from eq.(20).

5. Discussion

In the previous sections, we have developed a single-step method for PB-CT reconstruction of the 3D distribution of the complex refractive index in weakly scattering objects from multiple 2D transmission images collected in the Fresnel region (at some free-space propagation distance from the object) using coherent or partially-coherent incident X-ray beams at different illumination directions. It is instructive to summarise the assumptions that led us to the main results of this paper, eqs.(14), (20) as well as eqs.(32) and (33).

In order to derive eqs.(14) and (20) we made the following assumptions.

1. Plane fully-coherent incident wave, $U_{in}(\mathbf{r}) = I_{in}^{1/2} \exp(ikz)$, was assumed
2. Projection approximation was applied for the interaction of the incident wave with the object, eqs.(1) and (2).
3. Paraxial approximation (Fresnel diffraction) was assumed for the free-space propagation between the object and the detector, eq.(3).
4. Weak absorption in the object and Guigay's condition (slow variation) for the phase, eqs.(6), were assumed.

In order to derive eqs.(32) and (33), the assumptions 1 and 4 have been relaxed and replaced with the following assumptions.

5. Partially-coherent illumination of the object was assumed instead of the fully-coherent illumination.
6. In addition to the weak component, as in item 4 above, the attenuation function of the object was allowed to have a strong but slowly-varying component, eq.(26). This latter component of the attenuation function was assumed to be slowly varying on the length scale of the width of the 2D partially-coherent Fresnel propagator, $\tilde{P}_2^R(x', y) = (P_2^R * P_{sys})(x', y)$.

The single-step PB-CT reconstruction formulae, eqs.(22)-(23), have been derived under the above assumptions 1-4 in the case of a generic weakly-scattering object and two images per illumination direction collected at different object-to-detector distances and a range of illumination directions. We also gave a corresponding solution, eq.(24), for the 3D reconstruction of monomorphous objects from a single image per illumination direction. Similar equations can be easily derived from eq.(33) in the case of partially-coherent illumination and strongly absorbing samples satisfying the assumptions 5-6.

References

- M. A. Beltran, D. M. Paganin, K. Uesugi, and M. J. Kitchen, "2D and 3D X-ray phase retrieval of multi-material objects using a single defocus distance," *Opt. Express* **18**(7), 6423-6436 (2010).
- A. V. Bronnikov, "Reconstruction formulas in phase-contrast tomography," *Opt. Commun.* **171**, 239-244 (1999).

- A. V. Bronnikov, "Theory of quantitative phase-contrast computed tomography," *J. Opt. Soc. Am. A* **19**, 472-480 (1999).
- J. M. Cowley, *Diffraction physics*, 3rd ed. (North Holland Publishing Company, 1995).
- J. W. Goodman (2005), *Introduction to Fourier Optics*, 3rd ed. (Roberts & Company Publishers, 2005).
- J. P. Guigay, "Fourier transform analysis of Fresnel diffraction patterns and in-line holograms," *Optik* **49**, 121-125 (1977).
- J. P. Guigay, M. Langer, R. Boistel, and P. Cloetens, "Mixed transfer function and transport of intensity approach for phase retrieval in the Fresnel region," *Opt. Lett.* **32**, 1617-1619 (2007).
- T. E. Gureyev, D. Paganin, G. R. Myers, Y. I. Nesterets, and S. W. Wilkins, "Phase-and-amplitude computer tomography," *Appl. Phys. Lett.* **89**, 034102 (2006).
- T. E. Gureyev, A. Pogany, D. M. Paganin, and S. W. Wilkins, "Linear algorithms for phase retrieval in the Fresnel region," *Opt. Commun.* **231**, 53-70 (2004).
- T. E. Gureyev and Y. I. Nesterets, "Linear algorithms for phase retrieval in the Fresnel region. 3. Validity conditions," *Opt. Commun.* **405**, 394-399 (2017).
- S. C. Mayo, T. J. Davis, T. E. Gureyev, P. R. Miller, D. Paganin, A. Pogany, A. W. Stevenson, and S. W. Wilkins, "X-ray phase-contrast microscopy and microtomography," *Opt. Express* **11**, 2289-2302 (2003).
- F. Natterer, *The Mathematics of Computerized Tomography* (SIAM, 2001).
- Y. I. Nesterets and T. E. Gureyev, "Noise propagation in x-ray phase-contrast imaging and computed tomography," *J. Phys. D* **47**, 105402 (2014).
- Y. I. Nesterets and T. E. Gureyev, "Partially coherent contrast-transfer-function approximation," *J. Opt. Soc. Am. A* **33**, 464-474 (2016).
- D. Paganin, S. C. Mayo, T. E. Gureyev, P. R. Miller, and S. W. Wilkins, "Simultaneous phase and amplitude extraction from a single defocused image of a homogeneous object," *J. Microscopy* **206**, 33-40 (2002).
- D. M. Paganin, *Coherent X-Ray Optics* (Oxford University Press, 2006).
- A. Pogany, D. Gao, and S. W. Wilkins, "Contrast and resolution in imaging with a microfocus x-ray source," *Rev. Sci. Instrum.* **68**, 2774-2782 (1997).
- M. R. Teague, "Deterministic phase retrieval: a Green's function solution," *J. Opt. Soc. Am.* **73**(11), 1434-1441 (1983).

D. A. Thompson, Y. I. Nesterets, K. M. Pavlov, and T. E. Gureyev, “Fast three-dimensional phase retrieval in propagation-based X-ray tomography,” *J. Synchrotron Radiat.* **26**, 825–838 (2019).

X. Wu and H. Liu, “A general theoretical formalism for X-ray phase contrast imaging,” *J. X-Ray Sci. Technol.* **11**, 33–42 (2003).